Quantum Electronics **41** (8) 748–753 (2011)

NONLINEAR OPTICAL PHENOMENA

PACS numbers: 42.70.Qs; 42.65.Ky
DOI: 10.1070/QE2011v041n08ABEH014564

Deep-UV generation in an SBO crystal with an irregular domain structure

A.S. Aleksandrovsky, A.M. Vyunishev, A.I. Zaitsev, A.A. Ikonnikov, G.I. Pospelov, V.E. Rovskii, V.V. Slabko

Abstract. **Random (stochastic) quasi-phase matching is demonstrated for broadband radiation in a one-dimensional irregular strontium tetraborate nonlinear photonic crystal. Harmonic generation tunable in the range 187.5–215 nm is achieved. The average power of the generated signal is a quadratic function of pump power and reaches 1 μW. In a steady-state model, taking into account sum frequency generation within the spectrum of the input light causes no broadening of the peaks in the spectrum of the generated signal.**

Keywords: *second harmonic generation, random quasi-phase matching, nonlinear photonic crystal.*

1. Introduction

Nonlinear optical methods are commonly used to obtain laser radiation in different spectral regions. There are, however, insufficiently mastered spectral regions, e.g. the deep ultraviolet and, especially, the vacuum ultraviolet (VUV). This is primarily due to the limited number of crystalline nonlinear optical materials transparent in these spectral regions and to difficulties in angle phase matching. For example, phase-matched second harmonic generation (SHG) can be achieved at the shortest possible wavelength (204.8 nm) in beta barium borate (BBO) crystals. With known crystals, progression to shorter wavelengths is only possible through sum frequency generation, which adds great complexity to the experimental setup. In such cases, use is commonly made of high-power femtosecond laser systems with regenerative amplifiers and of a large number of nonlinear crystals, which leads to a necessity for time delay lines for pulse timing. The generation of light at wavelengths near 200 nm was analysed in detail by Petrov et al. [1].

From the viewpoint of mastering the VUV spectral region, there is considerable interest in strontium tetraborate (SBO) crystals, which possess the shortest wavelength limit of transmission, near 125 nm, among the known nonlinear optical crystals. Strontium tetraborate offers the largest nonlinear optical coefficients among the crystals transparent in the deep UV spectral region and has a high optical damage threshold. At the same time, angle phase matching for SHG is impossible in SBO crystals because of their low birefringence [2]. Nevertheless, the second harmonic signal in SBO crystals was reported to vary abnormally with light propagation direction [3], and the conversion efficiency was shown to be relatively high (up to 1%) [3, 4], which is atypical of phase-mismatched SHG. Recent work [5] has shown that SBO crystals tend to have an irregular domain structure. Such structures originate from the growth process and have the form of a stack of regions with an alternating static polarisation vector orientation and sign of second-order nonlinear susceptibility, which allows them to be regarded as nonlinear photonic crystals (NPCs) [6].

There is experimental evidence that such structures in SBO crystals allow random (stochastic) quasi-phase matching [7, 8] and nonlinear diffraction [9–11] to be realised. Predicted by Morozov et al. [12, 13] and first demonstrated experimentally by Baudrier-Raybaut et al. [14], random quasi-phase matching is intermediate in conversion efficiency between phase-mismatched harmonic generation and quasi-phase matching in regular domain structures (RDS's) [15, 16]. In the absence of phase matching, the power of the generated signal oscillates along the nonlinear medium with a period of two coherence lengths, whereas the power of the signal generated under quasi-phase matching conditions is a quadratic function of the number of domains. When domains are nonuniform in thickness, the generated signal increases on average linearly with distance in the medium [14, 17]. Conversion efficiency is then a weak function of the accuracy in crystal orientation and the spectral characteristics of the input light. Thus, the reduction in conversion efficiency is in this case the price to pay for tunability in wide spectral and angular ranges. In particular, this is basic to the possibility of measuring the duration of frequency-tunable ultrashort pulses at a fixed NPC position [18].

One well-established concept in the optics of linear photonic crystals is 'photonic band structure', which includes ranges of frequencies and tangential components of the wave vector where the propagation constant is either purely real-valued or complex-valued [19]. In connection with this, we proposed that the concept of band structure of linear photonic crystals should be extended to include NPCs [7]. Appropriate natural coordinates are then the incident radiation wavelength and angle of incidence. Therefore, the band structure of an NPC is a generalisation of the spectral and angular dependences of the generated signal and indicates the most efficient generation regions. In contrast to the band structure of photonic crystals, that of NPCs experiences a redshift [7]: generation efficiency remains unchanged when the wavelength of incident radiation

A.S. Aleksandrovsky, A.M. Vyunishev, A.I. Zaitsev L.V. Kirensky Institute of Physics, Siberian Branch, Russian Academy of Sciences, Akademgorodok 50/38, 660036 Krasnoyarsk, Russia; Siberian Federal University, Svobodnyi prosp. 79, 660041 Krasnoyarsk, Russia; e-mail: aleksandrovsky@kirensky.ru, vyunishev@iph.krasn.ru, az@iph.krasn.ru;
A.A. Ikonnikov, G.I. Pospelov, V.E. Rovskii, V.V. Slabko Siberian Federal University, Svobodnyi prosp. 79, 660041 Krasnoyarsk, Russia; e-mail: an_ton@pochtamt.ru, pospelovgi@mail.ru, filt-sfu@mail.ru, slabko@iph.krasn.ru

Received 17 February 2011; revision received 20 May 2011
Kvantovaya Elektronika **41** (8) 748–753 (2011)
Translated by O.M. Tsarev

and its angle of incidence are increased matchedly. Experimental evidence of such behaviour was presented in Ref. [20]. In this paper, we report an experimental study of femtosecond Ti:sapphire laser fourth harmonic generation in an SBO nonlinear photonic crystal under random quasi-phase matching conditions.

2. Theoretical model

Consider a one-dimensional irregular structure made up of N planar layers (domains) of homogeneous nonlinear material that is infinite in the (transverse) xy plane but has a finite thickness along the z axis. Adjacent domains differ only in the sign of a second-order nonlinear susceptibility tensor component. Let radiation of frequencies ω_i and ω_j propagate along the z axis and its electric field be linearly polarised in the plane of incidence. Assuming that the refractive index and its dispersion do not vary from domain to domain, we take that the second-order nonlinear susceptibility periodically switches sign from domain to domain. Then, in the harmonic plane wave approximation, when there is no pump depletion the amplitude of the field resulting from three-wave mixing ($\Omega_k = \omega_i + \omega_j$) within one domain of thickness d is given by

$$E_k = \frac{2\omega_i\omega_j\chi^{(2)}}{K'_k\Delta k_{ijk}} E_i E_j [\exp(\mathrm{i}\Delta k_{ijk} d) - 1],$$

where $\chi^{(2)}$ is a nonlinear susceptibility tensor component; $E_{i,j}$ is the optical field amplitude at frequencies $\omega_{i,j}$; $\Delta k_{ijk} = K'_k - k'_i - k'_j$ is the wave vector mismatch; and $k'_{i,j} = \omega_{i,j} n(\omega_{i,j})/c$ and $K'_k = \Omega_k n(\Omega_k)/c$ are the wave vectors of the incident and generated waves, respectively. Extending this approach to the entire structure, composed of alternating oppositely poled domains, we find the total amplitude of the field generated by all the domains when input light propagates inside the crystal at an angle θ' to the z axis:

$$E_{ijk} = \sum_{n=1}^{N} \left\{ \frac{2\omega_i\omega_j\chi_n^{(2)}}{K'_k(\theta')\Delta k_{ijk}(\theta')} E_i E_j \left[\exp\left(\mathrm{i}\Delta k_{ijk}(\theta')\frac{d_n}{\cos\theta'}\right) - 1 \right] \times \exp\left[\mathrm{i}\Delta k_{ijk}(\theta') \sum_{r=n+1}^{N} \frac{d_r}{\cos\theta'} \right] \right\}, \quad (1)$$

where n is the domain number; d_n is the thickness of the domain; and $\chi_n^{(2)} = (-1)^n|\chi^{(2)}|$ is its second-order nonlinear susceptibility. In (1), we performed the integration over each particular domain and the contributions of the domains are summed up with allowance for the different phase advances at the detection plane. Despite its apparent simplicity, this model ensures good agreement with experiment [7, 20]. The approach in question can be generalised to pulses with a broad spectrum. Let the spectrum of the incident light be Gaussian in shape: $E_{i,j}\exp[-(\omega_{i,j} - \omega_0)^2/\Delta\omega^2]$, where ω_0 is the centre frequency of the spectrum and $2\Delta\omega$ is its full 1/e width. The generated field strength corresponding to a particular spectral component has the form

$$E_k = \sum_{i=1}^{M} \sum_{j=k-i} \sum_{n=1}^{N} \left\{ \frac{2\omega_i\omega_j\chi_n^{(2)}}{K'_k(\theta')\Delta k_{ijk}(\theta')} \times E_i E_j \left[\exp\left(\mathrm{i}\Delta k_{ijk}(\theta')\frac{d_n}{\cos\theta'}\right) - 1 \right] \times \exp\left[\mathrm{i}\Delta k_{ijk}(\theta') \sum_{r=n+1}^{N} \frac{d_r}{\cos\theta'} \right] \right\}. \quad (2)$$

Here the summations are carried out over all $i,j = 1, 2, \ldots M$, with $k = i + j$. The use of Eqns (1) and (2) for calculating a nonlinear conversion in a particular sample requires knowledge of the thickness of all domains. Such information can be gained by optical or (in the case of thin domains) electron microscopy.

3. Experimental

The SBO sample studied, 5×11×9 mm in dimensions, had a domain structure 2.1 mm in length along the a crystallographic axis. The fact that the etching behaviour of SBO depends on the orientation of the static polarisation vector was used to visualise its domain structure. The domain structure was examined on a Carl Zeiss Axio Observer.Alm. It was made up of 262 domains, which ranged in thickness from tenths of a micron to tens of microns. The average domain size was 8 μm.

The pump source in our experimental fourth harmonic generation apparatus was a femtosecond Ti:sapphire laser tunable in the spectral range 720–960 nm. The average pump power was varied up to 960 mW, and the pulse duration was 40–100 fs. The pump beam was focused by an $f = 10$ cm lens into a 1-mm-thick BBO crystal. The second harmonic output was collimated by a similar lens. The average second harmonic power was up to 135 mW, which corresponded to a conversion efficiency of 14.4%. The second harmonic beam was isolated by a Glan prism and focused by an $f = 5$ cm lens into the centre of the NPC. The waist radius of the second harmonic beam at the $1/e^2$ intensity level was 37 μm, which corresponded to a peak power density of 0.3 GW cm^{-2}. The second harmonic signal was polarised along the c crystallographic axis, so that we used the largest nonlinear optical coefficient, d_{ccc}.

The fourth harmonic beam was focused onto the entrance slit of an MSDD 1000 monochromator equipped with a Hamamatsu HLS192 photodetector array for recording spectra. In the spectral range of interest, the spectral resolution of the monochromator was 0.023 nm (5 cm^{-1}). At the axial output of the monochromator was placed a Newport 918D detector connected to a Newport 1931-C power meter or Hamamatsu H5783-04 photomultiplier. In front of the monochromator, an Acton 172-N interference filter with a peak-transmission wavelength of 173.5 nm was placed (6.5% transmission at 200 nm). The average fourth harmonic power at the centre wavelength (200 nm) was up to 1 μW, which corresponded to a second to fourth harmonic conversion efficiency of 10^{-5}. The conversion efficiency reached in our experiments can be raised by at least two orders of magnitude with no optical breakdown.

4. Experimental results and discussion

Figure 1 shows the second and fourth harmonic spectra. The fourth harmonic spectrum was measured at normal incidence of the second harmonic beam on the NPC. The full width at half maximum of the second harmonic spectrum is 2.2 nm. The shape of the fourth harmonic spectrum is atypical of emission spectra obtained under angle phase matching conditions. In contrast to the (smooth) second harmonic spectrum, the fourth harmonic spectrum consists of sharp peaks, typically 1 Å in width, spaced 1–3 Å apart. Note that, in the spectral range under consideration, the calculated phase matching bandwidth corresponding to the first-order quasi-phase matching for SHG in RDS's would be just ~0.5 Å. The discrete nature

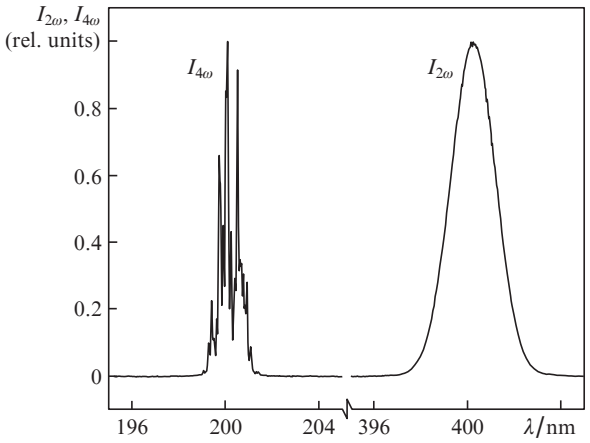

Figure 1. Normalised second and fourth harmonic spectra of a femtosecond laser.

of the spectrum suggests that the temporal shape of the generated pulses is distorted.

Figure 2a shows the measured spectra of the generated signal in the form of the spectral density diagram for the NPC rotated about the *b* crystallographic axis through angles from –30° to 30° in 1° steps at a fixed centre frequency of the incident light. As seen, rotation of the NPC shifts the spectral components to longer wavelengths within the pump spectrum, which allows the discrete structure in the fourth harmonic spectrum to be interpreted in terms of the band structure of the NPC [7]. The reason for this effect is that, with increasing incident radiation wavelength, the phase mismatch between the interacting waves is compensated through the increase in the optical thickness of the domains upon rotation of the NPC.

Figure 2b presents the results of NPC band structure calculations for the SHG process using Eqn (2) with allowance for the width of the pump spectrum. The calculations demonstrate that the angular dependence of the position of individual spectral components agrees well with the above experimental data. The use of the generalised formula (2) for calculating the spectrum of the generated signal causes no broadening of the peaks relative to the spectrum calculated by formula (1) [20]. The reason for this is that, with the dispersion that occurs in SBO crystals around the frequency of the incident light, the phase mismatch for a given spectral component of the generated signal is roughly the same for all possible combinations of components within the spectrum of the incident light.

Using the same approach as in the case of the diagram presented in Fig. 2b for the NPC, we calculated the spectral power density of the generated signal (Fig. 3a) for a single-domain sample 432 μm in thickness (in the process under consideration, this thickness equals 465 to 475 coherence lengths for different spectral components). The section through the

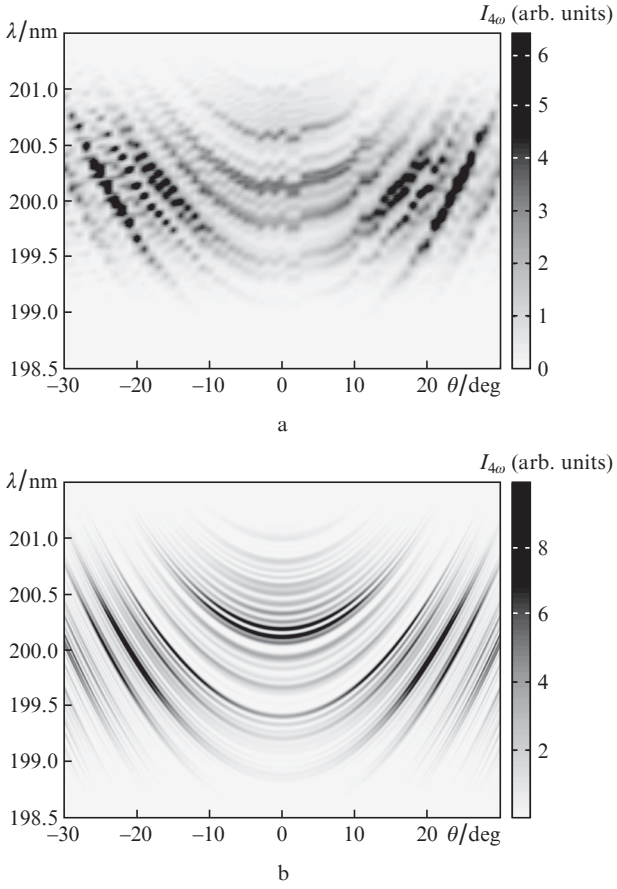

Figure 2. (a) Measured and (b) calculated angular dependences of the spectral power density of the signal generated near $\lambda = 200$ nm.

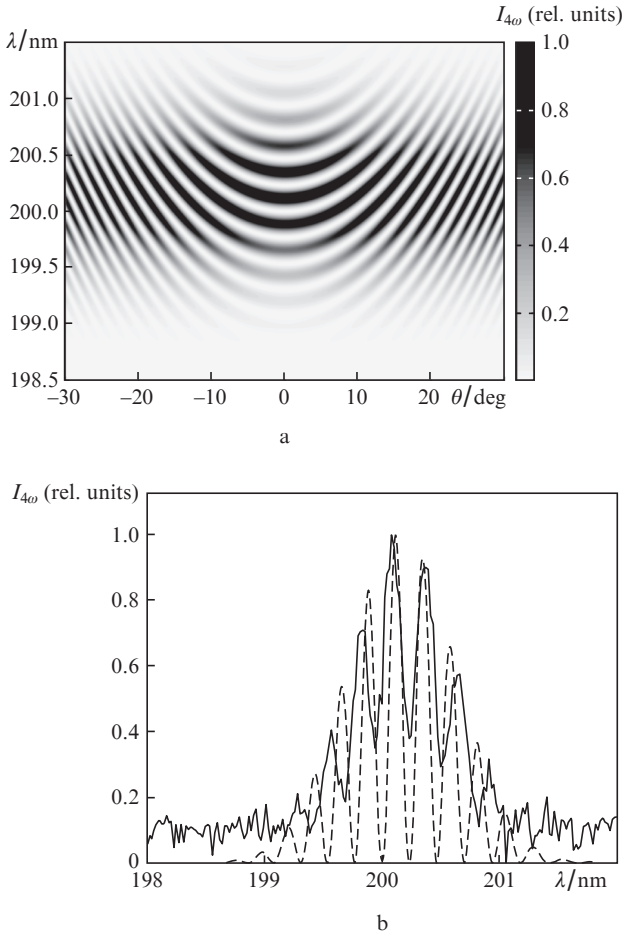

Figure 3. (a) Signal generated in a single-domain sample as a function of wavelength and angle. (b) Calculated (dashed line) and measured (solid line) normalised spectra of the signal generated in a single-domain sample at normal incidence of the input light.

diagram at a particular abscissa is the generated signal spectrum, which has the form of a frequency comb of evenly spaced peaks with a regularly shaped envelope, in agreement with experimental data (Fig. 3b). This behaviour is a spectral analogue of Maker's angular oscillations [21]. The slight discrepancy between the peaks in the calculated and measured spectra is most likely due to uncertainties in refractive index determination in the spectral region in question.

It is reasonable to quantify the increase in nonlinear conversion efficiency due to random quasi-phase matching by the ratio of the conversion efficiency in the NPC to that in a single-domain sample. When broadband radiation is converted in a randomised NPC, this ratio may vary widely over the generated signal spectrum. It is then reasonable to determine it using values integrated over the generated signal power spectra of the NPC and single-domain sample. As a reference, we used a single-domain sample 432 μm thick along the *a* crystallographic axis, with its *c* crystallographic axis parallel to the polarisation of the second harmonic beam. The increase in conversion efficiency due to random quasi-phase matching was by a factor of 320, which is of the same order as the calculated value. The latter is, however, about a factor of 800 lower than the value calculated for first-order quasi-phase matching in an RDS of the same thickness as the NPC under consideration. The marked reduction in conversion efficiency is the price to pay for tunability in a wide spectral range.

Varying the centre wavelength of the input light, we obtained tunable femtosecond Ti:sapphire laser fourth harmonic generation in an SBO NPC in the range 187.5–215 nm (Fig. 4). The main factors that determine the short-wavelength limit of the tuning range are the absorption in air and the tuning curve of the pump laser, whereas the absorption in the SBO has only a secondary effect. In the absorption spectrum of the NPC, we identified a peak at 209 nm, with an absorption coefficient of 0.6 cm^{-1} (0.45 cm^{-1} at 200 nm). According to Oseledchik et al. [4], absorption in this range is unrelated to the main components of SBO. It seems likely that this feature is due to unintentional impurities. Consequently, such impurities can be eliminated by improving the purity of starting materials and utilising a procedure that precludes contamination of the melt during crystal growth.

Figure 5 shows the average power of the signal generated in the NPC as a function of pump power. The data are sufficiently well represented by a quadratic curve, just as in the cases of angle phase matching and quasi-phase matching [22]. This lends support to the simple model represented by (2). Moreover, this means that, at pump intensities above 0.3 GW cm^{-2}, the power of the short-wavelength signal would be expected to increase considerably.

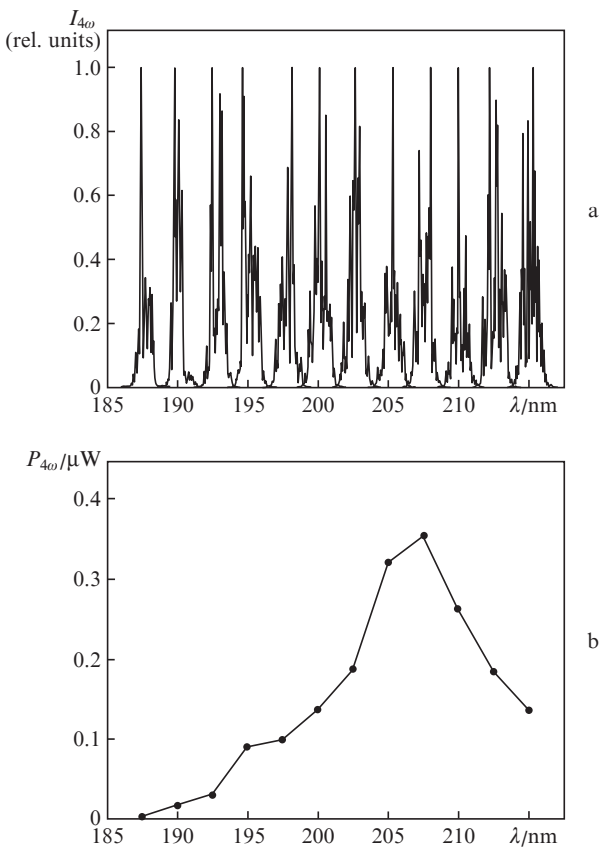

Figure 4. (a) Normalised fourth harmonic spectra of a femtosecond laser at different centre wavelengths of the pump radiation. (b) Average fourth harmonic power $P_{4\omega}$ vs. output centre wavelength.

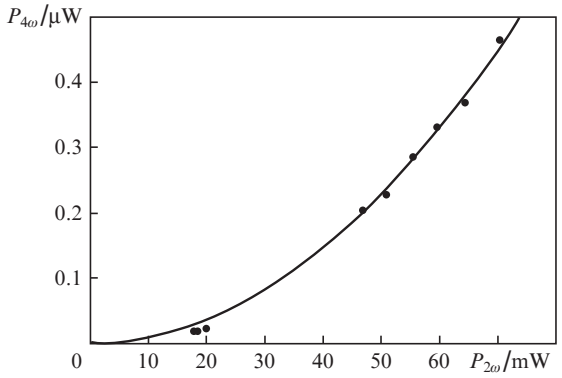

Figure 5. Measured average fourth harmonic power, $P_{4\omega}$, as a function of average second harmonic power, $P_{2\omega}$.

One distinctive feature of nonlinear optical conversion in NPCs is associated with the direction of light propagation through their domain structure. Clearly, the sequences of domains differ in thickness in such cases. At the same time, from the viewpoint of the output signal these structures are equivalent because they have one spectrum of reciprocal lattice vectors. The equivalence can be illustrated by calculation using Eqn (2) (Fig. 6). It follows from Fig. 6 that the spectra of the signal generated in such structures for opposite propagation directions of the input light will vary in different ways, but the result will be the same. In this process, the peaks in the spectrum of the generated signal become narrower.

In addition, the spectrum-integrated power is independent of the light propagation direction (Fig. 7a). To experimentally verify this conjecture, we measured spectra of the generated signal for the forward and reverse propagation directions of the pump light. In this process, we optimised the maximum power of the generated signal by varying the position of the focal spot in the NPC. As seen in Fig. 7b, the spectrum of the generated signal is independent of the input light propagation direction in the NPC structure and the position of the NPC. The latter suggests that the domain structure is highly ordered in the crystallographic plane *bc*. From the observed reduction in the power of the generated signal by 15% when pump light was passed first through the NPC structure and then through

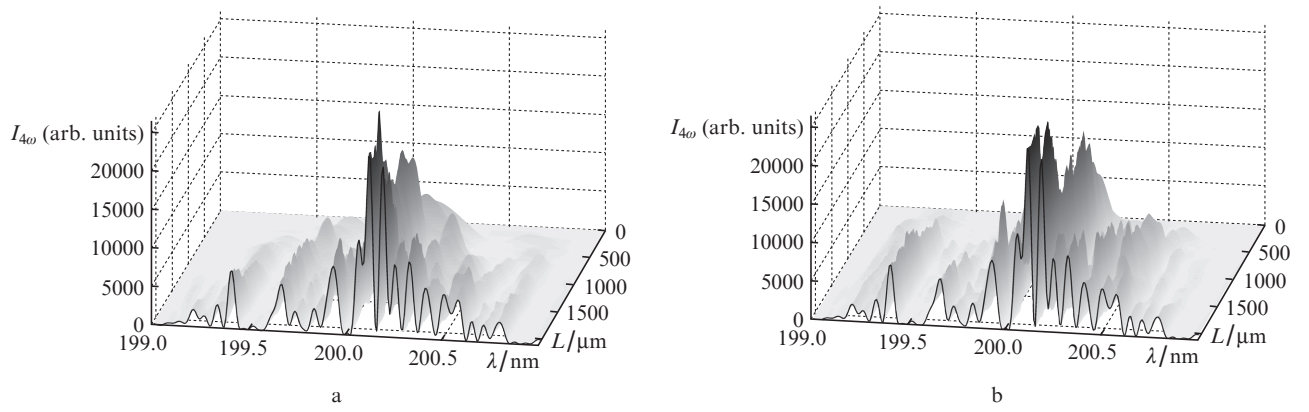

Figure 6. Evolution of the signal generated in an NPC along its domain structure in the (a) forward and (b) reverse directions.

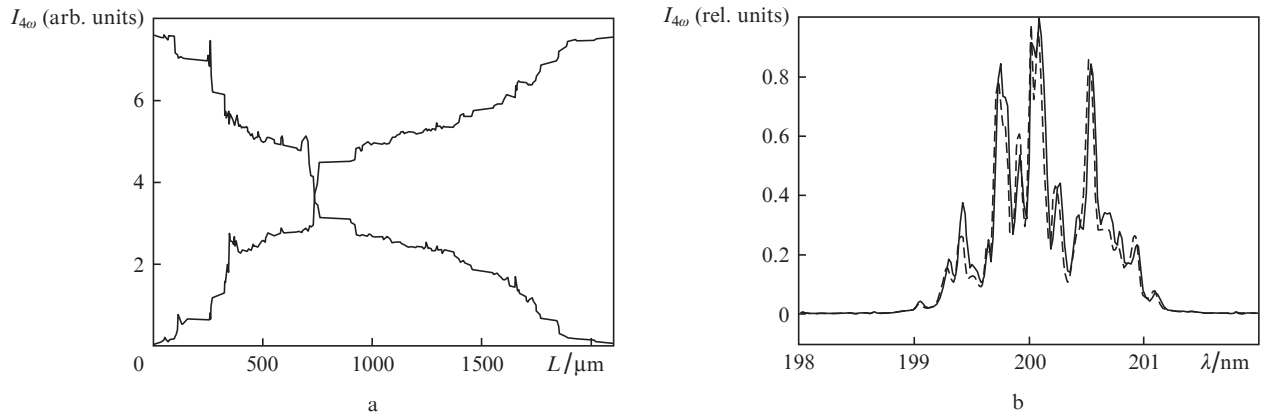

Figure 7. (a) Calculated integrated power at the fourth harmonic frequency as a function of input light propagation direction. (b) Normalised spectra of the signal generated in an NPC for the forward (solid line) and reverse (dashed line) propagation directions of the pump light.

an extended single-domain region, the absorption coefficient of the NPC material at 200 nm was estimated at 0.54 cm^{-1}. This value correlates well with the absorption spectra of the NPC and a 432-μm-thick SBO plate.

The calculation results in Fig. 7a can be used to assess the inhomogeneity of the NPC. Even though the increase in the integrated intensity of the generated signal can on the whole be considered roughly linear, there are regions where the intensity rises considerably more steeply in comparison with the entire structure. This suggests that future advances in the technology of SBO NPCs will ensure an increase in conversion efficiency not only through an increase in pump intensity, as discussed above, but also through a more favourable domain thickness distribution.

5. Conclusions

Tunable (187.5–215 nm) cascade femtosecond Ti:sapphire laser fourth harmonic generation has been demonstrated using random quasi-phase matching in an SBO NPC. The spectrum-integrated increase in conversion efficiency due to random quasi-phase matching was by a factor of 320 relative to phase-mismatched generation in a single-domain sample. The highest average fourth harmonic power was 1 μW. The power of the generated signal was shown to be a quadratic function of pump power. In a steady-state model, taking into account sum frequency generation within the spectrum of the input light causes no broadening of the peaks in the spectrum of the generated signal. SBO nonlinear photonic crystals that ensure random quasi-phase matching can serve as a basis for angle- and wavelength-noncritical nonlinear optical conversion tunable over the vacuum ultraviolet spectral region.

Acknowledgements. This work was supported by the RF Ministry of Education and Science (State Contract No. 16.740.11.0150), the RF President's Grants Council (Support to Leading Scientific Schools Programme, Grant No. NSh-4645.2010.2), the Federal Agency for Education (Grant No. RNP.2.1.1.3455, Project Nos 2.5.2 and 3.9.1), the Siberian Branch of the Russian Academy of Sciences (Project Nos 27.1 and 5), the Krasnoyarsk Krai Foundation for Support to Scientific and Technological Activities, and Carl Zeiss, Inc.

References

1. Petrov V., Rotermund F., Noack F., Ringling J., Kittelmann O., Komatsu R. *IEEE J. Sel. Top. Quantum Electron.*, **5**, 1532 (1999).
2. Grechin S.S., Pryalkin V.I. *Kvantovaya Elektron.*, **33**, 737 (2003) [*Quantum Electron.*, **33**, 737 (2003)].
3. Pan F., Shen G., Wang R., Wang X., Shen D. *J. Cryst. Growth*, **241**, 108 (2002).
4. Oseledchik Yu.S., Prosvirnin A.L., Pisarevskiy A.I., Starshenko V.V., Osadchuk V.V., Belokrys S.P., Svitanko N.V., Korol A.S., Krikunov S.A., Selevich A.F. *Opt. Mater.*, **4**, 669 (1995).
5. Zaitsev A.I., Aleksandrovsky A.S., Vasiliev A.D., Zamkov A.V. *J. Cryst. Growth*, **310**, 1 (2008).
6. Berger V. *Phys. Rev. Lett.*, **81**, 4136 (1998).

7. Aleksandrovsky A.S., Vyunishev A.M., Shakhura I.E., Zaitsev A.I., Zamkov A.V. *Phys. Rev. A*, **78**, 031802-1 (2008).
8. Aleksandrovsky A.S., Vyunishev A.M., Shakhura I.E., Zaitsev A.I., Zamkov A.V. *Opt. Spektrosk*., **107**, 384 (2009).
9. Aleksandrovsky A.S., Vyunishev A.M., Zaitsev A.I., Zamkov A.V., Arkhipkin V.G. *J. Opt. A*, **9**, S334 (2007).
10. Aleksandrovsky A.S., Vyunishev A.M., Slabko V.V., Zaitsev A.I., Zamkov A.V. *Opt. Commun*., **282**, 2263 (2009).
11. Vyunishev A.M., Aleksandrovsky A.S., Cherepakhin A.V., Rovskii V.E., Zaitsev A.I., Zamkov A.V. *Kratk. Soobshch. Fiz*., **37**, 85 (2010).
12. Morozov E.Yu., Kaminskii A.A., Chirkin A.S., Yusupov D.B. *Pis'ma Zh. Eksp. Teor. Fiz*., **73**, 731 (2001).
13. Morozov E.Yu., Chirkin A.S. *Kvantovaya Elektron*., **34**, 227 (2004) [*Quantum Electron*., **34**, 227 (2004)].
14. Baudrier-Raybaut M., Haïdar R., Kupecek Ph., Lemasson Ph., Rosencher E. *Nature*, **432**, 374 (2004).
15. Fejer M.M., Magel G.A., Jundt D.H., Byer R.L. *IEEE J. Quantum Electron*., **28**, 2631 (1992).
16. Dmitriev V.G., Tarasov L.V. *Prikladnaya nelineinaya optika* (Applied Nonlinear Optics) (Moscow: Fizmatlit, 2004).
17. Vidal X., Martorell J. *Phys. Rev. Lett.*, **97**, 013902-1-013902-4, (2006).
18. Aleksandrovsky A.S., Vyunishev A.M., Zaitsev A.I., Ikonnikov A.A., Pospelov G.I. *Appl. Phys. Lett.*, **98**, 061104, (2011).
19. Yariv A., Yeh P. *Optical Waves in Crystals* (New York: Wiley, 1984; Moscow: Mir, 1987).
20. Aleksandrovsky A.S., Vyunishev A.M., Zaitsev A.I., Slabko V.V. *Phys. Rev. A*, **82**, 055806 (2010).
21. Maker P.D., Terhune R.W., Nisenoff M., Savage C.M. *Phys. Rev. Lett.*, **8**, 21 (1962).
22. Kravtsov N.V., Laptev G.D., Naumova I.I., Novikov A.A., Firsov V.V., Chirkin A.S. *Kvantovaya Elektron.*, **32**, 923 (2002) [*Quantum Electron.*, **32**, 923 (2002)].